Characterization and Performance Comparison of Ripple-Based Control for Voltage Regulator Modules

Jian Sun, *Member, IEEE*

***Abstract*—Three recently developed control methods for voltage regulator modules, namely, V^2 control, enhanced V^2 control, and enhanced V^2 control without output voltage dynamic feedback, are analyzed and compared in this paper. All three methods utilize the output voltage switching ripple for pulse-width modulation (PWM), hence, are collectively referred to as ripple-based control. A general modeling method based on the Krylov–Bogoliubov–Mitropolsky ripple estimation technique is applied to develop averaged models for single-channel as well as multichannel buck converters employing each of the control methods. Unlike existing models that are limited to small-signal operation, the proposed models are valid for large-signal operation and are capable of predicting subharmonic instability without including any sample-and-hold block as used in previous models. The paper also shows that adding parallel, high-quality ceramic capacitors at the output, which are ignored in previous models, can lead to pulse skipping and ripple instability, and a solution based on proper selection of the ceramic capacitors and/or ramp compensation at the PWM is presented. The models are further applied to analyze and compare the performance of the three control methods in terms of ripple stability, effective load current feedforward gain, and output impedance.**

***Index Terms*—Averaged modeling, enhanced V^2 control, load current feedforward, ripple-based control, ripple estimation, ripple instability, V^2 control, voltage regulator modules (VRMs), VRM control.**

I. Introduction

MODERN microprocessors and other high-speed digital integrated circuits (ICs) require low-voltage, high-current power supplies, referred to as voltage regulator modules (VRMs) in the literature. Output voltage regulation, particularly under dynamic load current switching, is the most important performance measurement for VRMs. Conventional control methods such as current-mode and voltage-mode control [1] rely on fast feedback loops for output voltage regulation, which have major limitations in meeting the stringent transient response requirements of future VRMs [1].

Recently, several new control methods, namely, V^2 control [2], [3], enhanced V^2 control [4], [5], and enhanced V^2 control without output voltage dynamic feedback [6], have been proposed to improve the speed of VRM transient responses to load current switching. All three methods utilize the switching-frequency ripple of converter output voltage for pulse-width modulation (PWM), hence, are collectively referred to as ripple-based control in this paper. These methods improve VRM responses to load current switching by virtue of inherent load current feedforward through the equivalent series resistance (ESR) of the output capacitors. Performance advantages of these methods over conventional current- and voltage-mode control have been demonstrated [2]–[6].

As with any other control method, proper models are needed for understanding and designing VRM with ripple-based control. Small-signal models for each of the mentioned ripple-based control methods have been reported in previous works [2]–[6]. These models were derived through direct applications of the PWM model developed for peak-current control [7]. The original PWM model presented in [7] cannot predict subharmonic instability under peak-current control and when the duty ratio exceeds 50%. To remedy this deficiency, a second-order transfer function representing the so-called sample-and-hold (S&H) effect was added to the modulator model. This additional second-order transfer function is included in all existing models for ripple-based control [2]–[6] without justification.

Existence of the S&H effect in a PWM process and the necessity to include it in average-based PWM converter models have been a subject of debate for some time now. The primary reason for considering the S&H effect in [7] was to enable the resulting model to predict subharmonic instability. However, the averaged models presented in [8] and [9] didn't consider any S&H effect, yet they are able to correctly predict the subharmonic instability, which indicates that the S&H effect does not need to be considered when modeling peak-current control as far as subharmonic instability prediction is concerned. On the other hand, the existing models without the second-order S&H transfer function, although much simpler, are not able to predict subharmonic instability under ripple-based control.

Another limitation of the existing models is that they all assume, implicitly, that the output voltage ripple is dominated by the voltage across the output capacitor ESR, and that the ESR ripple voltage is piece-wise linear over time (referred to as linear ripple hereafter) and proportional to the inductor ripple current, in which case the modulation process closely resembles that of peak-current control. Linear ripple would be a valid assumption when only bulk filter capacitors with identical time constants ($\tau = r_C C$) and relatively high ESR are used. In practical designs, however, low-ESR, high quality ceramic capacitors are always used in parallel with bulk capacitors to im-

Manuscript received May 25, 2004; revised October 14, 2005. This work was supported in part by the Center for Power Electronics Systems (CPES) (an Engineering Research Center of the National Science Foundation). This work was presented in part at the IEEE Power Electronics Specialists Conference, Aachen, Germany, June 2004. Recommended by Associate Editor F. Blaabjerg.

The author is with the Department of Electrical, Computer, and Systems Engineering, Rensselaer Polytechnic Institute, Troy, NY 12180-3590 USA (e-mail: jsun@rpi.edu)

Digital Object Identifier 10.1109/TPEL.2005.869747

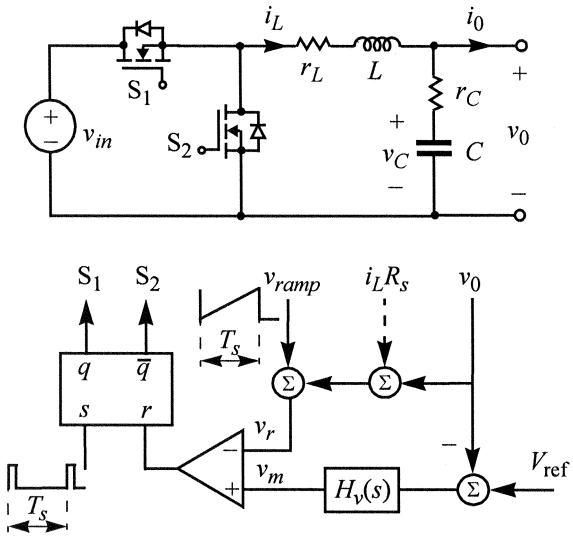

Fig. 1. Synchronous buck converter with V^2 control. The sensed current signal, $i_L R_s$, is only used in enhanced V^2 control.

prove the filtering effectiveness at high frequencies. These additional capacitors, although small in capacitance, can significantly alter the waveform of the ripple voltage such that it is no longer piece-wise linear over time and proportional to the inductor ripple current. Direct application of the peak-current control modulator model, which relies on linear ripple assumption, would result in erroneous models in this case for ripple-based control.

This paper presents a different modeling approach for VRM with ripple-based control. It is an extension of the method introduced in [8] for modeling peak-current control. A more detailed overview of the method will be given in Section II following a review of different ripple-based control methods. The inherent load current feedforward mechanism common in all ripple-based control is also examined. Section III presents the application of the modeling method when the output voltage ripple is linear. Section IV extends the method to converters with nonlinear output voltage ripple, that is, when low-ESR, ceramic capacitors are used in parallel with bulk output filter capacitors. It will also be shown there that the nonlinear ripple can lead to pulse skipping and ripple instability under V^2 control, and that the problem can be avoided by limiting the capacitance of low-ESR capacitors and/or by incorporating a compensation ramp. The developed models are validated by numerical simulation and experimental measurement results in Section V. The models are also used to study the performance of the control methods, and the concept of load current feedforward is further examined in conjunction with output impedance analysis. Section VI concludes the paper.

II. Ripple-Based Control and Modeling

A. V^2 Control

The basic principle of V^2 control [2] as applied to a single-channel buck converter is illustrated in Fig. 1. The inverted input to the PWM comparator is a combination of the converter output voltage, v_0, and a compensation ramp, v_{ramp}. The third signal,

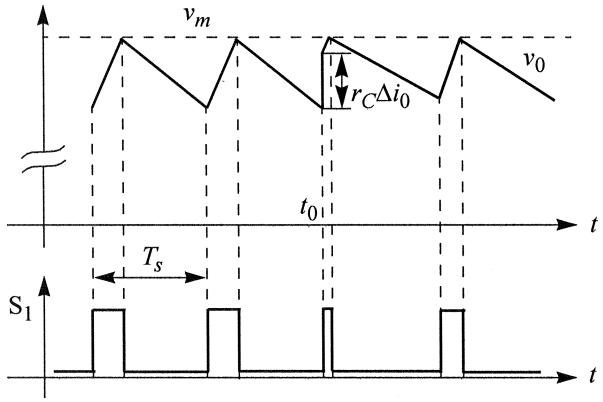

Fig. 2. Duty ratio response of V^2 control to a load current step-down change.

$i_L R_s$, represents the sensed inductor current and is used in enhanced V^2 control but not in V^2 control. Operation of the modulator relies on the switching-frequency ripple at the output of the converter. Similar to peak-current control, all ripple-based control methods have subharmonic instability problem, as will be discussed later in the paper. The purpose of adding the compensation ramp, v_{ramp}, is to avoid subharmonic instability when the duty ratio of S_1 exceeds 50%.

In steady-state operation, the dc component (average) of the inductor current is equal to the load current such that there is no dc current through the ESR, r_C, of the capacitor. Under the assumption that the load resistance is much higher than the ESR of the capacitor, almost all of the inductor ripple current, $\hat{i}_L$, will be absorbed by the capacitor. Furthermore, the ripple component of v_C (defined in Fig. 1) is very small and can be ignored. Under these conditions, the output voltage ripple is simply the ripple voltage across the ESR, which is equal to the inductor ripple current times r_C

$$\hat{v}_0 = r_C \hat{i}_L. \tag{1}$$

Therefore, steady-state operation of V^2 control is similar to that of peak-current control, with the ESR of the output capacitor acting as a sensing resistor for the inductor current.

However, transient response of V^2 control, particularly to load current switching, is fundamentally different from that of peak-current control. Consider, for example, a step-down change in the load current as illustrated in Fig. 2. Assume that the load current is reduced by Δi_0 at $t = t_0$. Since the inductor current cannot change instantaneously, the average of the inductor current will exceed the load current by Δi_0 in a short time period following the load current change. The current through the capacitor ESR will be the inductor ripple current plus Δi_0 in this time period. As such, the output voltage will have a step change equal to $r_C \Delta i_0$ at t_0, as illustrated in Fig. 2. This will cause an immediate decrease in the switch duty ratio, which has the effect to reduce the inductor current and to reestablish the balance between the inductor current and the load current. Note that the switch duty ratio is reduced here without the intervention of the voltage control loop. In contrast, under peak-current control, the duty ratio will only change when the voltage compensator has detected the variation of the output voltage and starts to adjust its output, v_m. The speed of

response in that case depends primarily on the design of the voltage feedback control loop and will be much slower.

The fast response of V^2 control to load current switching can be attributed to its inherent load current feedforward mechanism. As is apparent from the foregoing discussion, any mismatch between the inductor current and the load current will be reflected in the voltage across r_C, which immediately affects the duty ratio. If the peak-to-peak inductor ripple current is ΔI_{pk}, the feedforward gain from the load current to the duty ratio can be found from Fig. 2 as (assume there is no ramp compensation)

$$K_{ff} = \frac{\Delta d}{\Delta i_0} = \frac{D}{\Delta I_{pk}} \tag{2}$$

where D is the duty ratio before the load current changes. Since the inductor current ripple, ΔI_{pk}, is small, a small variation in i_0 can change the duty ratio by a very large amount. In fact, it can be determined from (2) that a decrease in i_0 by the amount of ΔI_{pk}, or an increase in i_0 by the amount of

$$\Delta i_0 = \frac{1-D}{D} \cdot \Delta I_{pk}$$

will immediately saturate the modulator (duty ratio becomes 0 or 1, respectively), thereby providing the highest possible slew rate for the inductor current.

B. Other Ripple-Based Control Methods

Enhanced V^2 control [4], [5] differs from V^2 control in that the inductor current is sensed and added to the inverted input to the PWM, as shown by the dashed line in Fig. 1. This has the effect of reducing the sensitivity of duty ratio response to output voltage noise and the variation of the capacitor ESR, but at the expense of reduced load current feedforward gain. With the inductor current sensed by a resistor, R_s, the load current feedforward gain under enhanced V^2 control is found to be

$$K_{ff} = \frac{\Delta d}{\Delta i_0} = \frac{D}{\Delta I_{pk}} \cdot \frac{r_C}{R_s + r_C} \tag{3}$$

which is lower than that under V^2 control, see (2). The lower feedforward gain will lead to increased output impedance, as the analysis in Section V will show.

A simplified version of the enhanced V^2 control was presented in [6]. Its basic control structure is essentially identical to that of enhanced V^2 control, except that the voltage feedback controller, represented by $H_v(s)$ in Fig. 1, is removed and that the reference voltage, $V_{\rm ref}$, is connected directly to the noninverted input to the modulator. As the analysis in Section V will show, the output impedance of a VRM under enhanced V^2 control and without a voltage feedback loop open has a relatively flat magnitude and close to -180° phase response, which closely resembles that of a resistor as required by adaptive output voltage regulation for VRM [12]. Therefore, removing the output voltage dynamic controller can be beneficial for transient response of the converter output voltage to load current switching.

C. Modeling Method

The modeling method applied here is an extension of that developed for modeling peak-current control [8]. In this approach, a complete model for a VRM consists of an averaged model of the power stage and a duty ratio constraint that defines the duty

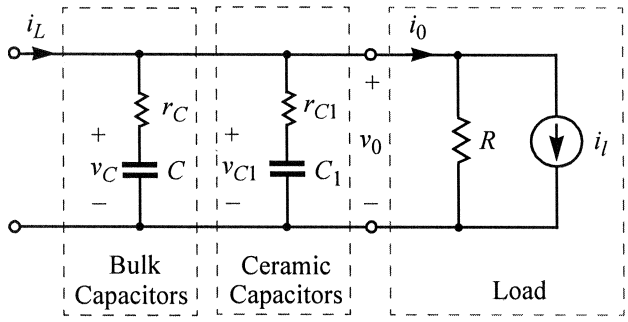

Fig. 3. Output section and load of a buck converter with two different types of filter capacitors. Branch r_C–C represents the bulk filter capacitors, while r_{C1}–C_1 represents the parallel, low-ESR, ceramic capacitors. The load is modeled by a resistor, R, in parallel with a current source, i_l.

ratio in the form of an algebraic equation. Averaged modeling of a buck converter is straightforward. In order for the model to be as general as possible, we assume that the load consists of a resistor, R, in parallel with a current source, i_l. Under continuous conduction mode of the inductor, the state-space averaged model of a single-channel buck converter is simply

$$\begin{aligned} \frac{d\bar{i}_L}{dt} &= \frac{dv_{\rm in} - \bar{i}_L r_L}{L} + \frac{(i_l - \bar{i}_L)Rr_C - R\bar{v}_C}{(R+r_C)L} \\ \frac{d\bar{v}_C}{dt} &= \frac{(\bar{i}_L - i_l)R - \bar{v}_C}{(R+r_C)C} \end{aligned} \tag{4}$$

where $\bar{i}_L$ and $\bar{v}_C$ is the average of the inductor current (i_L) and the capacitor voltage (v_C), respectively. Discontinuous conduction mode of the inductor, although not considered here, can be modeled using the method presented in [13].

State-space averaging can also be applied to model multichannel buck converters. The result will be a $(n+1)$-order averaged model, with n being the number of interleaved channels. If the n channels are assumed to have identical circuit and control parameters, the averaged model can be simplified into a second-order system given below, where L and r_L is the inductance and ESR of the inductor in each channel, and $\bar{i}_L$ represents the total averaged inductor current of n channels combined

$$\begin{aligned} \frac{d\bar{i}_L}{dt} &= \frac{dv_{\rm in} - \frac{\bar{i}_L r_L}{n}}{\frac{L}{n}} + \frac{(i_l - \bar{i}_L)Rr_C - R\bar{v}_C}{\frac{(R+r_C)L}{n}} \\ \frac{d\bar{v}_C}{dt} &= \frac{(\bar{i}_L - i_l)R - \bar{v}_C}{(R+r_C)C}. \end{aligned} \tag{5}$$

Equation (5) can also be expanded to account for additional, low-ESR ceramic capacitors in parallel with the bulk filter capacitors. The multiple ceramic capacitors can be modeled by a single branch consisting of the total effective ESR, r_{C1}, and capacitance, C_1, as shown in Fig. 3. With this the state-space averaged model of the converter with n interleaved channels can be written as follows where L and r_L are defined as in (5):

$$\begin{aligned} \frac{d\bar{i}_L}{dt} &= \frac{dv_{\rm in} - \frac{\bar{i}_L r_L}{n}}{\frac{L}{n}} + \frac{(i_l - \bar{i}_L)Rr_C r_{C1} - R(r_{C1}\bar{v}_C + r_C\bar{v}_{C1})}{\frac{[r_C r_{C1} + R(r_C + r_{C1})]L}{n}} \\ \frac{d\bar{v}_C}{dt} &= \frac{(\bar{i}_L - i_l)Rr_{C1} - (R+r_{C1})\bar{v}_C + R\bar{v}_{C1}}{[r_C r_{C1} + R(r_C + r_{C1})]C} \\ \frac{d\bar{v}_{C1}}{dt} &= \frac{(\bar{i}_L - i_l)Rr_{C1} + R\bar{v}_C - (R+r_C)\bar{v}_{C1}}{[r_C r_{C1} + R(r_C + r_{C1})]C}. \end{aligned} \tag{6}$$

To complete the averaged model (4)–(6), a duty ratio constraint relating d to other variables is needed. Note that the duty ratio is defined by the inverted input to the modulator, which can be written as

$$v_r(t) = v_{\text{ramp}}(t) + R_s i_L(t) + v_0(t) \tag{7}$$

where R_s is zero under V^2 control. Note that $i_L(t)$ and $v_0(t)$ in (7) represent the instantaneous value of the inductor current and the output voltage, not their average. Since the averaged models (4)–(6) do not involve these instantaneous quantities, they have to be replaced by other variables used in the averaged models. A mathematical tool that can be used for this purpose is the Krylov–Bogoliubov–Mitropolsky (KBM) method [10], [11].

Application of the KBM method requires lengthy and tedious algebraic calculations and manipulations of both the original piece-wise linear model and the averaged model. To solve this problem, a symbolic analysis program package, SYMAP [14], was developed in Mathematica [15] by the author a few years ago to automate the derivation of ripple functions for PWM converters. By using this package, the first-order inductor current and capacitor voltage ripple of a single-channel buck converter are calculated to be [8]

$$\hat{i}_L(t) = \frac{v_{\text{in}}}{2L} \cdot \begin{cases} (d-1)(dT_s - 2t) & t \in [0, dT_s] \\ d[(1+d)T_s - 2t] & t \in [dT_s, T_s] \end{cases} \tag{8}$$

$$\hat{v}_C(t) = 0 \tag{9}$$

where T_s denotes the length of a switching cycle. Similar functions are obtained for n-channel buck converters, as given in the following, where L is the inductance of each channel. The expressions below are valid for the first one-n^{th} of a switching cycle, $t \in [0, T_s/n]$, in which the first channel is turned on and off once while all other channels remain off.

1) First Channel:

$$\hat{i}_{L1}(t) = \frac{v_{\text{in}}}{2L} \cdot \begin{cases} (d-1)(dT_s - 2t) & t \in [0, dT_s] \\ d[(1+d)T_s - 2t] & t \in \left[dT_s, \frac{T_s}{n}\right] \end{cases}. \tag{10}$$

2) All Other Channels:

$$\hat{i}_{Lk}(t) = \frac{v_{\text{in}}}{2L} \cdot d\left[(1+d)T_s - 2\left(t + \frac{k-1}{n}T_s\right)\right]. \tag{11}$$

3) Output Capacitor Ripple Voltage:

$$\hat{v}_C(t) = 0. \tag{12}$$

According to the analysis, ESR of the inductors and the capacitors have no effects on the KBM ripple expressions given so far. Also, note that the capacitor ripple voltage is zero in all cases. This result is consistent with the fact that the current through the output capacitor in a buck converter is continuous and, hence, its voltage does not have first-order ripple.

With known first-order ripple of the inductor current and capacitor voltage, $i_L(t)$ and $v_C(t)$ can be approximated by $\bar{i}_L + \hat{i}_L(t)$ and $\bar{v}_C + \hat{v}_C(t)$, respectively, from which the actual output voltage, $v_0(t)$, can also be determined. Since the two inputs to the modulator are equal at the time when the switch turns off, the duty ratio has to satisfy the following duty ratio constraint in general

$$v_r(dT_s) = v_m. \tag{13}$$

Note that v_m is a slowly varying variable (or constant in the case when no dynamic voltage feedback is used), hence can be considered a constant over a switching cycle.

III. Modeling Under Linear Ripple Conditions

The output ripple voltage, $\hat{v}_0$, is piece-wise linear over time and proportional to the inductor ripple current if only bulk filter capacitors with identical time constants are used.

A. Single-Channel Buck

Since capacitor C (without its ESR) has no first-order ripple [see (9)], the instantaneous output voltage including its ripple component can be written as

$$v_0(t) = \bar{v}_C + r_C\left[\hat{i}_L(t) + C\frac{d\bar{v}_C}{dt}\right] \tag{14}$$

where $\hat{i}_L(t)$ is defined by (8). The derivative term in (14) represents the nonripple voltage across r_C when the internal capacitor voltage, v_C, is not in steady state, that is, when the average of inductor current is different from the load current. Using (4), (7), (8), and (13), noting $i_L(t) = \bar{i}_L + \hat{\hat{i}}_L(t)$, and assuming that the ramp signal has a slope equal to m_c, i.e., $v_{\text{ramp}}(t) = m_c t$ for $t \in [0, T_s]$, we found that (13) can be written out as follows for enhanced V^2 control:

$$m_c dT_s + R_s\bar{i}_L + \bar{v}_C + r_C \cdot \frac{(\bar{i}_L - i_l)R - \bar{v}_C}{R + r_C} + \frac{v_{\text{in}}}{2L} \cdot (r_C + R_s)(1-d)dT_s = v_m. \tag{15}$$

The duty ratio constraint (15) combined with the state-space averaged model (4) forms a complete, large-signal averaged model for single-channel buck converter with enhanced V^2 control. With R_s set to zero, (15) becomes the duty ratio constraint for V^2 control.

B. Multichannel Interleaved Buck

In an n-channel buck converter, the current i_L that flows into the output section of the converter (see Fig. 3) is the sum of all n inductor currents. The output voltage in this case can still be calculated by using (14), but the ripple current $\hat{i}_L(t)$ there has to be the total ripple of all n channels combined

$$\hat{i}_L(t) = \sum_{k=1}^{n} \hat{i}_{Lk}(t) \tag{16}$$

where $\hat{i}_{Lk}(t)$ is the ripple current of the k^{th} channel as defined by (10) and (11). On the other hand, inductor current of the k^{th}-channel will only be used by its own modulator under enhanced V^2 control, that is, the inverted input to the modulator of the k^{th}-channel is defined by

$$v_{rk}(t) = v_{\text{ramp},k}(t) + R_s i_{Lk}(t) + v_0(t). \tag{17}$$

Without losing generality, let's consider the first channel, for which the compensation ramp can be written as $v_{\text{ramp},1}(t) = m_c t$ over each switching cycle. Based on (5), (10), (11), (16),

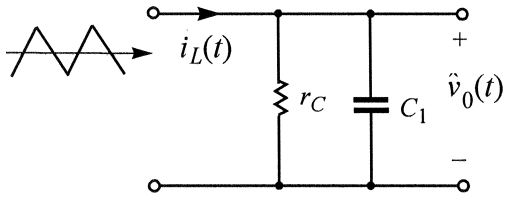

Fig. 4. Approximate circuit for calculation of the output voltage ripple when low-ESR, ceramic capacitors are used.

and (17), the duty ratio constraint (13) under enhanced V^2 control can be written out as follows:

$$\frac{R_s\bar{i}_L}{n}+\bar{v}_C+r_C\cdot\frac{(\bar{i}_L-i_l)R-\bar{v}_C}{R+r_C}+m_cdT_s +\frac{v_{\text{in}}}{2L}\cdot dT_s[R_s(1-d)+r_C(1-nd)]=v_m. \quad (18)$$

As in (5), $\bar{i}_L$ in (18) is the total average inductor current of n channels combined. Equation (18) together with (5) forms a complete averaged model for n-channel buck converter with enhanced V^2 control. For V^2 control, a duty ratio constraint can be obtained from (18) by setting R_s to zero.

IV. Modeling Under Nonlinear Ripple Conditions

The output voltage ripple can no longer be assumed piece-wise linear and proportional to the inductor ripple current when low-ESR, ceramic capacitors are used in parallel with bulk filter capacitors. Effects of nonlinear ripple on performance of ripple-based control and their modeling are discussed below.

A. Ripple Voltage and Duty Ratio Constraints

With the piece-wise linear inductor current ripple defined by (8), or (10) and (11), the output voltage ripple could be calculated based on the second-order circuit shown in Fig. 3. However, to simplify the calculation, we will use the approximate circuit shown in Fig. 4, in which the load is treated as an open circuit, the ESR of the ceramic capacitors is ignored, and the bulk capacitors are modeled by their ESR only. The approximations are justified considering frequency characteristics of each part of the circuit.

Since single channel can be considered a special case of n-channel with $n=1$, the following discussions will focus on n-channel converters. The results are applicable to single-channel converters by simply setting n to 1. With reference to Fig. 4, the output ripple voltage $\hat{v}_0(t)$ is calculated in three steps.

1) Assume an arbitrary initial value for $\hat{v}_0(t)$ at the beginning of a switching cycle and calculate the response of the circuit in Fig. 4 over a ripple period, $[0, T_s/n]$. The input to the circuit is the ripple current $\hat{i}_L(t)$.
2) Since we are interested in periodical response of the ripple, the value of $\hat{v}_0(t)$ at $t=T_s/n$ can be assumed to be equal to its initial value: $\hat{v}_0(T_s/n)=\hat{v}_0(0)$. This relationship can be used to determine the actual initial value of $\hat{v}_0(t)$ at the beginning of a ripple period.
3) The calculated initial value of $\hat{v}_0(t)$ can now be substituted into the general solution to complete the definition for the output ripple voltage over a ripple period, $[0, T_s/n]$.

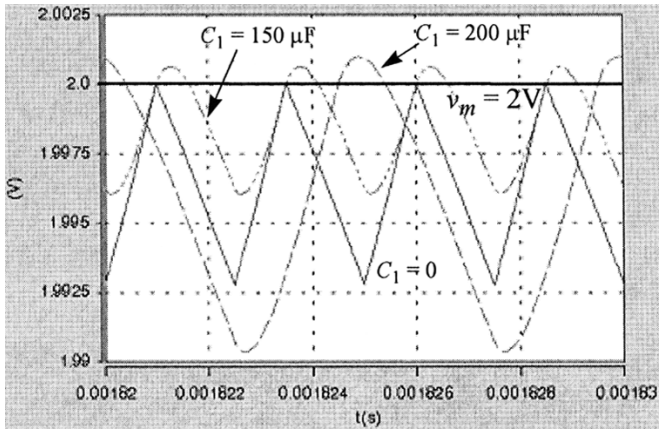

Fig. 5. Output voltage ripple under V^2 control and with different number of ceramic capacitors in parallel with bulk filter capacitors.

The calculated initial value, $\hat{v}_0(0)$, and the response of $\hat{v}_0(t)$ in the interval $[0, dT_s/n]$, which is what is needed for the duty ratio constraint, are given in the Appendix. With these, the inverted input to channel-one modulator can be written as

$$\begin{aligned}v_{r1}(t)&=v_{\text{ramp},1}(t)+R_si_{L1}(t)+\bar{v}_0+\hat{v}_0(t)\\&=m_ct+R_s\left[\frac{\bar{i}_L}{n}+\hat{i}_{L1}(t)\right]+\left[\bar{v}_C+r_CC\frac{d\bar{v}_C}{dt}\right]+\hat{v}_0(t)\end{aligned}$$

from which a duty ratio constraint is obtained by using (6), (10), and the expression for $\hat{v}_0(t)$ given in the Appendix :

$$m_cdT_s+\frac{R_s\bar{i}_L}{n}+\frac{v_{\text{in}}}{2L}\cdot dT_s(1-d)R_s+\hat{v}_0(dT_s) +\bar{v}_C+\frac{(\bar{i}_L-i_l)Rr_{C1}-(R+r_{C1})\bar{v}_C+R\bar{v}_{C1}}{\left[r_{C1}+R\left(1+\frac{r_{C1}}{r_C}\right)\right]C}=v_m. \quad (19)$$

This can be combined with (6) to form a complete average model for n-channel buck converters with enhanced V^2 control. The model can be used for single-channel converters if n is set to 1, and for V^2 control if R_s is set to zero.

B. Pulse Skipping and Mitigation

Fig. 5 shows the output voltage ripple waveform with different capacitance C_1. The waveforms were obtained by numerical simulation using SABER for a converter with V^2 control that will be further defined in the next subsection. No compensation ramp was used for any of the simulation results. As can be seen, the ripple voltage is piece-wise linear when no ceramic capacitors are used ($C_1=0$). With $C_1=150$ μF (15 × 10-μF ceramic capacitors in parallel), the ripple voltage becomes smaller, but also very nonlinear. The switching frequency is stable and is 400 kHz in both cases. When C_1 is further increased to 200 μF, however, the modulator starts to skip pulses so the switching frequency changes to 200 kHz. As the result, the ripple voltage also increases significantly.

The pulse skipping problem as observed from Fig. 5 is caused by the lagging phase of the output voltage ripple relative to the inductor current ripple. Due to this lagging phase, the ripple voltage continues to rise after the switch is turned off, i.e., when the inductor current already starts to decreases, as can be seen from Fig. 5 for the case with $C_1=150$ μF. With a large C_1,

TABLE I
POWER STAGE PARAMETERS OF THE TWO-CHANNEL TEST VRM

V_{in} (V)	L (μH)	C (μF)	r_C (mΩ)	C_1 (μF)	T_s (μs)
5	0.825	7000	3.4	120	3

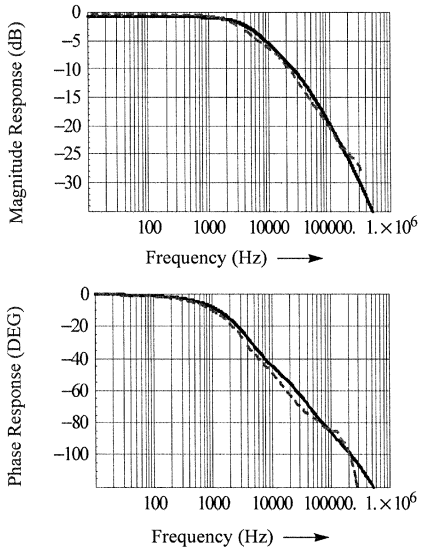

Fig. 6. Control-to-output frequency responses of the test VRM. Solid lines: model prediction; dashed lines: experimental measurements.

the ripple voltage may lag the ripple current so much that it is still higher than v_m (shown to be 2 V in Fig. 5) by the end of a switching cycle, in which case the switch will not turn on at all in the following switching cycle, leading to pulse skipping. This is what happened in the case of $C_1 = 200$ μF shown in Fig. 5.

Since the lagging phase of the ripple voltage is related to the time constant $r_C C_1$, pulse skipping can be avoided by selecting C_1 such that $r_C C_1$ is insignificant compared to a ripple cycle, T_s/n. Simulation results have shown that no pulse skipping would occur if $r_C C_1$ doesn't exceed 10% of T_s/n. Also note that, under enhanced V^2 control and/or when a compensation ramp is used, the additional linear ripple component(s) would dominate v_r such that larger ceramic capacitors may be used without running into the pulse skipping problem.

V. MODEL VALIDATION AND ANALYSIS

A two-channel, enhanced V^2-controlled VRM demo board from On Semiconductor [16] has been used as the basis for validation of the models developed in the preceding sections as well as for the analysis and performance comparison between the three control methods. Main parameters of the power stage of the converter are given in Table I.

A. Control-to-Output Characteristics

Operation of the converter with 5-V input, 1.7-V output, and with a resistive load, $R = 0.147\ \Omega$, was measured. In particular, the control-to-output frequency responses were measured and are shown in Fig. 6. Meantime, the control-to-output transfer function, $V_0(s)/v_m(s)$, of the converter was calculated through linearization of the power stage model (6) in conjunction with the duty ratio constraint (19). Frequency responses of the resulting transfer function was plotted in Fig. 6 for comparison with the experimental results. As can be seen, the measurement results agree very well with model predictions up to 200 kHz, which is about 1/3 of the output ripple frequency (2 × 335 kHz). Note that the ESR value (3.4 mΩ) given in Table I represents the maximal ESR provided in the data sheet; the model prediction uses half of the maximal value. Losses of the converter are accounted for by including in the model an additional, 17-mΩ resistor in series with the inductor.

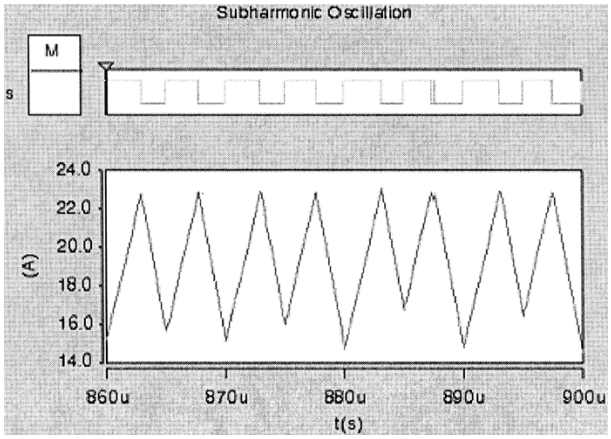

Fig. 7. Subharmonic oscillation in a single-channel buck converter with enhanced V^2 control. The duty ratio should be 0.56 under stable operation.

The control-to-output response under V^2 control is similar to that shown in Fig. 6, but the unity gain extends to almost half the switching frequency, particularly when no compensation ramp is used. The response is similar to the inductor current response under peak-current control. Detailed analysis can be performed using the models derived before and is omitted here due to space limit.

B. Subharmonic Instability and Prediction

Another similarity between ripple-based control and peak-current control is the subharmonic instability problem: Without a compensation ramp, $v_{\rm ramp}$, the converter experiences subharmonic oscillation when the duty ratio exceeds 50%. This occurs in both V^2 control and enhanced V^2 control, and is the primary reason for the use of the compensation ramp. Fig. 7 shows SABER simulation results of a single-channel buck converter with enhanced V^2 control that shows subharmonic oscillation in both the gate signal (upper trace) and the inductor current (lower trace). Parameters of the converter are the same as those given in Table I except that the switching frequency is 400 kHz and that only bulk filter capacitors are used.

To predict the subharmonic oscillation, the existing models have to include a second-order transfer function as part of the modulator gain [3]–[6], which significantly increases the complexity of the model. In contrast, the models developed in Sections III–IV are directly capable of predicting subharmonic instability. To demonstrate this, we consider a V^2-controlled single-channel buck converter with only bulk output filter capacitors. As discussed before, (4) and (15) form a large-signal averaged model of the converter in this case. To determine small-signal stability of the converter, the system matrix of the

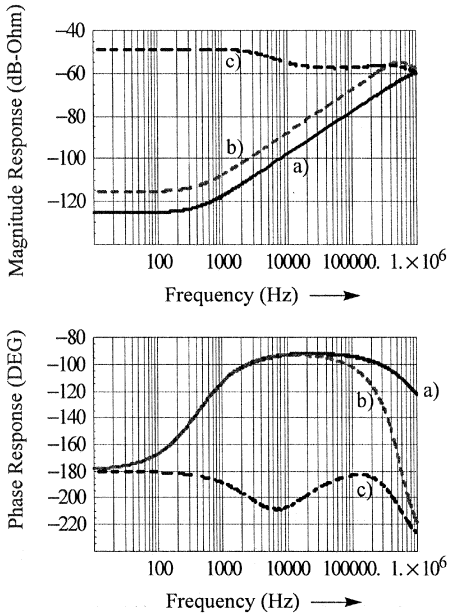

Fig. 8. Open-loop output impedance comparison for a two-channel buck converter: (a) V^2 control with only bulk output filter capacitors, (b) V^2 control with 120-μF ceramic capacitors in parallel with the bulk capacitors, and (c) enhanced V^2 control with $R_s = 7.7$ mΩ.

linearized version of this averaged model was calculated and is given as

$$\mathbf{A} = \begin{bmatrix} \frac{-2}{T_s(1-2d)} & -\frac{2L+(1-2d)r_C T_s}{(1-2d)LrC T_s} \\ \frac{1}{C} & -\frac{1}{RC} \end{bmatrix}. \tag{20}$$

To simplify the expression, the compensation ramp is set to zero and ESR of the inductor and the capacitor is ignored in the power stage model (but included in the duty ratio constraint). It can be shown that one of the eigenvalues of matrix $\mathbf{A}$ becomes positive if $1-2d$ is negative. This indicates that the small-signal model becomes unstable when the duty ratio exceeds 50%, which is consistent with what SABER simulation results showed. The ability to predict subharmonic instability using pure algebraic modulator gain is a major advantage of the proposed modeling method.

As with peak-current control, subharmonic instability under ripple-based control can also be eliminated by adding a compensation ramp to the modulator input. Selection of the compensation ramp is similar to that for peak-current control and can be done based on the averaged model presented in this paper. For simulation results shown in Fig. 7, for example, analysis of the model indicated that adding a 1.5-mV/μs compensation ramp would stabilize the converter.

C. Output Impedance

Output impedance is the most important performance measure for VRM. The large-signal averaged models presented in Sections III–IV provide a basis for the analysis of output impedance under various operation conditions. Due to the limited space, only one set of results are included (see Fig. 8) which shows the frequency responses of the output impedance of a two-channel buck converter without a voltage compensator, i.e., with a constant v_m. Parameters of the converter power stage are the same as those given in Table I. To avoid subharmonic oscillation, a 3 mV/μs compensation is used. Three different responses are given:

a) V^2 control with only bulk output filter capacitors, that is, without the 120-μF ceramic capacitors;
b) V^2 control with both bulk output filter capacitors and the 120-μF ceramic capacitors;
c) Enhanced V^2 control with both bulk output filter capacitors and the 120-μF ceramic capacitors. The effective inductor current sensing gain is 7.7 mΩ.

It is interesting to note that the parallel ceramic capacitors actually increases the output impedance, which is caused by the reduction in the effective load current feedforward gain when ceramic capacitors are added. The plots also show that the output impedance response under enhanced V^2 control is almost purely resistive (flat magnitude, -180° phase). A resistive output is most desirable for meeting adaptive output voltage regulation requirements for VRM [12], and Fig. 8 shows that this might be achieved by enhanced V^2 control without using any dynamic voltage feedback, an idea that is behind the work presented in [6].

Through adjustment of the control parameters, the output impedance under enhanced V^2 control could be made to more closely emulate a resistor. Of particular interests is the possibility to completely eliminate the dynamics of the output impedance by, e.g., adding dynamic compensation elements to the load current feedforward path. This requires a load current signal separate from the output voltage and the inductor current ripple, which could be generated indirectly by using a series RL or RC current sensing circuit connected in parallel with the output capacitor, based on the same principle as that for sensing the inductor current [17]. This will be addressed in a future work.

VI. Conclusion

Ripple-based control for voltage regulator modules achieves fast transient response to load current switching by virtue of inherent load current feedforward. Compared to V^2 control, enhanced-V^2 control has lower load current feedforward gain due to the addition of the inductor current at the modulator input, and the converter behaves more like that with peak-current control as the inductor current gain increases. Both V^2 and enhanced-V^2 control have subharmonic instability problem when the duty ratio exceeds 50%, of which the mechanism is similar to that under peak-current control. Use of low-ESR, ceramic capacitors in parallel with bulk output filter capacitors results in nonlinear output voltage ripple, which can lead to pulse skipping and reduced switching frequency if the time constant formed by the capacitance of ceramic capacitors and the ESR of bulk filter capacitors is comparable to one ripple period.

A general modeling method based on ripple estimation using the KBM algorithm was proposed. The method can be applied to develop large-signal averaged models for single-channel and multi-channel VRM's employing each of the ripple-based control methods. The resulting models are capable of predicting subharmonic instability and are much simpler, both conceptually and mathematically, than existing models incorporating a sample-and-hold transfer function. Various transfer functions can be determined from a linearized version of the large-signal averaged models, and the small-signal models are found to be

accurate up to half the switching frequency. Of particular interests is the output impedance under enhanced-V^2 control when no voltage dynamic feedback is used: The open-loop output impedance response closely resembles that of a resistor, which can be exploited to meet adaptive voltage regulation requirements for VRM. The analysis also pointed to possible performance improvement through more sophisticated load current feedforward control design.

APPENDIX

The initial value of the output voltage ripple component, $\hat{v}_0(t)$, at the beginning of each ripple period ($[0, T_s/n]$) and its response during the on-time of the switch, $[0, dT_s]$, are calculated using the procedure outlined in Section IV-A. The results are as follows ($\tau = r_C C_1$, $\alpha = T_s/\tau$):

$$\hat{v}_0(0) = \frac{-r_C V_{\text{in}}}{2L(e^{\alpha/n}-1)} \cdot [d(1-nd)T_s(e^{\alpha/n}-1)+2\tau(nd-1+e^{d\alpha}-de^{\alpha/n})]$$

$$\hat{v}_0(t) = \hat{v}_0(0)e^{-t/\tau} + \frac{V_{\text{in}} r_C(1-nd)}{2L} \cdot [2t+(2\tau+dT_s)(e^{-t/\tau}-1)], \qquad t \in [0, dT_s].$$

REFERENCES

[1] J. Sun, "Control design considerations for voltage regulator modules," in *Proc. IEEE Int. Telecommun. Energy Conf. (INTELEC'03)*, Oct. 2003, pp. 84–91.

[2] D. Gorder and W. R. Pelletier, "V^2 architecture provides ultra fast transient response in switch mode power supplies," in *Proc. HFPC'96 Conf.*, 1996, pp. 19–23.

[3] S. Qu, "Modeling and design considerations of V^2 controlled buck regulator," in *Proc. IEEE APEC'01 Conf.*, 2001, pp. 507–513.

[4] W. Huang and J. Clarkin, "Analysis and design of multiphase synchronous buck converter with enhanced V^2 control," in *Proc. HFPC'00 Conf.*, 2000, pp. 74–81.

[5] W. Huang, "A new control for multi-phase buck converter with fast transient response," in *Proc. IEEE APEC'01 Conf.*, 2001, pp. 273–279.

[6] K. Lee, K. Yao, X. Zhang, Y. Qiu, and F. C. Lee, "A novel control method for multiphase voltage regulators," in *Proc. IEEE APEC*, 2003, pp. 738–743.

[7] R. B. Ridley, "A new, continuous-time model for current-mode control," *IEEE Trans. Power Electron.*, vol. 6, no. Apr., pp. 271–280, Apr. 1991.

[8] J. Sun and R. M. Bass, "A new approach to average modeling of PWM converters with current-mode control," in *Proc. IEEE IECON'97 Conf.*, 1997, pp. 599–604.

[9] F. D. Tan and R. D. Middlebrook, "A unfied model for current-programmed converters," *IEEE Trans. Power Electron.*, vol. 10, no. 4, pp. 397–408, Jul. 1995.

[10] N. N. Bogoliubov and Y. A. Mitropolsky, *Asymptotic Methods in the Theory of Nonlinear Oscillations*. New Delhi, India: Hindustan Publishing Corp., 1961.

[11] R. M. Bass, "Large-signal tools for power electronics: State-space analysis and averaging theory," Ph.D. dissertation, Univ. Illinois, Urbana-Champaign, 1990.

[12] *Voltage Regulator-Down (VRD) Design Guide 10.0*, Intel Corporation, 2004.

[13] J. Sun *et al.*, "Averaged modeling of PWM converters operating in discontinuous conduction mode," *IEEE Trans. Power Electron.*, vol. 6, no. 4, pp. 482–4922, Jul. 2001.

[14] J. Sun and H. Grotstollen, "Symbolic analysis methods for averaged modeling of switching power converters," *IEEE Trans. Power Electron.*, vol. 12, no. 3, pp. 537–546, May 1997.

[15] S. Wolfram, *The Mathematica Book*. Champaign, IL: Wolfram Media, 1996.

[16] *Demonstration Note for CS5308*, On Semiconductor, 2002.

[17] C. Chen, "Combined lossless current sensing for current mode control," in *Proc. IEEE Applied Power Electron. Conf.*, 2004, pp. 404–410.

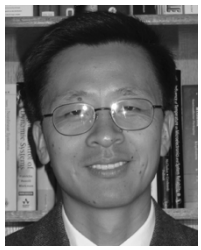

Jian Sun (M'95) received the B.S. degree from the Nanjing Institute of Aeronautics, Nanjing, China, in 1984, the M.S. degree from the Beijing University of Aeronautics and Astronautics, Beijing, China, in 1989, and the Ph.D. degree from the University of Paderborn, Paderborn, Germany, in 1995, all in electrical engineering.

He was a Post-Doctoral Fellow in the School of Electrical and Computer Engineering, Georgia Institute of Technology, Atlanta, from 1996 to 1997, where he taught undergraduate courses on electromechanical energy conversion. He worked in the Advanced Technology Center of Rockwell Collins, Inc., from 1997 to 2002, where he led several projects on the development of various power conversion technologies for aerospace applications. In August 2002, he joined the Department of Electrical, Computer, and Systems Engineering, Rensselaer Polytechnic Institute, Troy, NY, as an Associate Professor. He has published more than 70 journal and conference papers on these subjects, and holds four U.S. patents, with several more pending. His research interests are in the general area of power electronics and energy conversion, with particular emphasis on converter topologies, modeling, control, and various applications including computers, communications, aerospace, and energy systems.

Dr. Sun is a Member of the IEEE Power Electronics Society. He currently serves as an Associate Editor for IEEE POWER ELECTRONICS LETTERS. He is the Vice Chairman of the IEEE Power Electronics Society's Technical Committee on Simulation, Modeling, and Control, and the General Chair of IEEE COMPEL'06 Workshop.